

Estimating Depth from Monocular Images as Classification Using Deep Fully Convolutional Residual Networks

Yuanzhouhan Cao, Zifeng Wu, Chunhua Shen

Abstract—Depth estimation from single monocular images is a key component in scene understanding. Most existing algorithms formulate depth estimation as a regression problem due to the continuous property of depths. However, the depth value of input data can hardly be regressed exactly to the ground-truth value. In this article, we propose to formulate depth estimation as a pixel-wise classification task. Specifically, we first discretize the continuous ground-truth depths into several bins and label the bins according to their depth ranges. Then we solve the depth estimation problem as classification by training a fully convolutional deep residual network. Compared to estimate the exact depth of a single point, it is easier to estimate its depth range. More importantly, by performing depth classification instead of regression, we can easily obtain the confidence of a depth prediction in the form of probability distribution. With this confidence, we can apply an information gain loss to make use of the predictions that are close to ground-truth during training, as well as fully-connected conditional random fields (CRF) for post-processing to further improve the performance. We test our proposed method on both indoor and outdoor benchmark RGB-D datasets and achieve state-of-the-art performance.

V Conclusion 9

References 9

CONTENTS

I	Introduction	2
II	Related Work	2
III	Proposed Method	3
III-A	Network architecture	3
III-B	Loss function	4
III-C	Fully connected conditional random fields	4
IV	Experiments	5
IV-A	Depth label classification vs. depth value regression	5
IV-B	Component evaluation	7
IV-B1	Benefit of information gain matrix	7
IV-B2	Benefit of fully connected CRFs	7
IV-B3	Network Comparisons	7
IV-C	State-of-the-art comparisons	7
IV-C1	NYUD2	8
IV-C2	KITTI	8
IV-C3	Cross-dataset evaluation	8

Y. Cao, Z. Wu and C. Shen are with The University of Adelaide, School of Computer Science, Australia. (email:{yuanzhouhan.cao, zifeng.wu, chunhua.shen}@adelaide.edu.au.)

I. INTRODUCTION

Depth estimation is one of the most fundamental tasks in computer vision. Many other computer vision tasks such as object detection, semantic segmentation, scene understanding, can benefit considerably from accurate estimation of depth information. Most existing methods [1], [2], [3], [4] formulate depth estimation as a structured regression task due to the fact of depth values being continuous. These regression models for depth estimation are trained by iteratively minimizing the L_2 norm between the predicted depths and the ground-truth depths, and aim to output depths as close to the actual depths as possible during evaluation. However, it is difficult to regress the depth value of input data to be exactly the ground-truth value. For human beings, we may find it difficult to tell the exact distance of a specific point in a natural scene, but we can easily give a rough distance range of that point. Motivated by this, we formulate depth estimation as a pixel-wise classification task by discretizing the continuous depth values into several discrete bins. Instead of training a model to predict the depth value of a point, we train a model to predict the depth range. We show that this simple re-formulation scheme performs surprisingly well.

Another important reason for us to choose classification over regression for depth estimation is that it naturally predicts a confidence in the form of probability distribution over the output space. Different points have different distributions of possible depth values. The depth estimation of some points are easy while others are not. Typical regression models only output the mean values of possible depth values without the variances, (i.e., the confidence of a prediction is missing). Some efforts have been made to obtain this confidence such as the constrained structured regression [5], or the Monte-Carlo dropout [6], [7]. Compared to these methods which either require specific constraints or multiple forward passes during evaluation, our proposed approach is simple to implement.

The obtained probability distribution can be an important cue during both training and post-processing. Although we formulate depth estimation as a classification task by discretization, the depth labels are different from the labels of typical classification tasks such as semantic segmentation. During training, the predicted depth labels that are close to ground-truth and with high confidence can also be used to update model parameters. This is achieved by an information gain loss. As for the post-processing, we apply the fully-connected conditional random fields (CRF) [8] which have been frequently applied in semantic segmentation [9], [10]. With the fully connected CRFs, pixel depth estimation with low confidence can be improved by other pixels that are connected to it.

Traditional depth estimation methods enforce geometric assumptions and rely on hand-crafted features such as SIFT, PHOG, GIST, texton, etc. Recently, computer vision has witnessed a series of breakthrough results introduced by deep convolutional neural networks (CNN) [11], [12]. The success of deep networks can be partially attributed to the rich features captured by the stacked layers. Recent evidence has shown that depth estimation benefits largely from increased number

of layers [13], [1], [4]. However, stacking more layers does not necessarily improve performance as the training can become very difficult due to the problem of vanishing gradients. In this work, we apply the the deep residual learning framework proposed by He et al. [14]. It manages to learn the residual mapping of a few stacked layers to avoid the vanishing gradients problem.

An overview of our proposed depth estimation model is illustrated in Fig. 1. It takes as input an arbitrarily sized image and outputs a dense score map. Fully connected CRFs are then applied to obtain the final depth estimation. The remaining content of the paper is organized as follows. Section II reviews some relevant work. Then we present the proposed method in Section III. Experiment results are presented in Section IV. Finally, Section V concludes the paper.

II. RELATED WORK

Previous depth estimation methods are mainly based on geometric models. For example, the works of [15], [16], [17] rely on box-shaped models and try to fit the box edges to those observed in the image. These methods are limited to only model particular scene structures and therefore are not applicable for general-scene depth estimations. More recently, non-parametric methods [18] are explored. These methods consist of candidate images retrieval, scene alignment and then depth inference using optimizations with smoothness constraints. These methods are based on the assumption that scenes with semantically similar appearances should have similar depth distributions when densely aligned.

Other methods attempt to exploit additional information. To name a few, the authors of [19] estimated depths through user annotations. The work of [20] performed semantic label prediction before depth estimation. The works of [21], [3] have shown that jointly perform depth estimation and semantic labelling can help each other. Given the fact that the extra source of information is not always available, most of recent works formulated depth estimation as a Markov Random Field (MRF) [22], [23], [24] or Conditional Random Field (CRF) [25] learning problem. These methods managed to learn the parameters of MRF/CRF in a supervised fashion from a training set of monocular images and their corresponding ground-truth depth images. The depth estimation problem then is formulated as a maximum a posteriori (MAP) inference problem on the CRF model.

With the popularity of deep convolutional neural networks (CNN) since the work of [11], some works attempted to solve the depth estimation problem using deep convolutional networks and achieved outstanding performance. Eigen et al. [1] proposed a multi-scale architecture for predicting depths, surface normals and semantic labels. The multi-scale architecture is able to capture many image details without any superpixels or low-level segmentation. Liu et al. [4] presented a deep convolutional neural field model for depth estimation. It learned the unary and pairwise potentials of continuous CRF in a unified deep network. The model is based on fully convolutional networks (FCN) with a novel superpixel pooling method. Similarly, Li et al. [2] and Wang et al. [3]

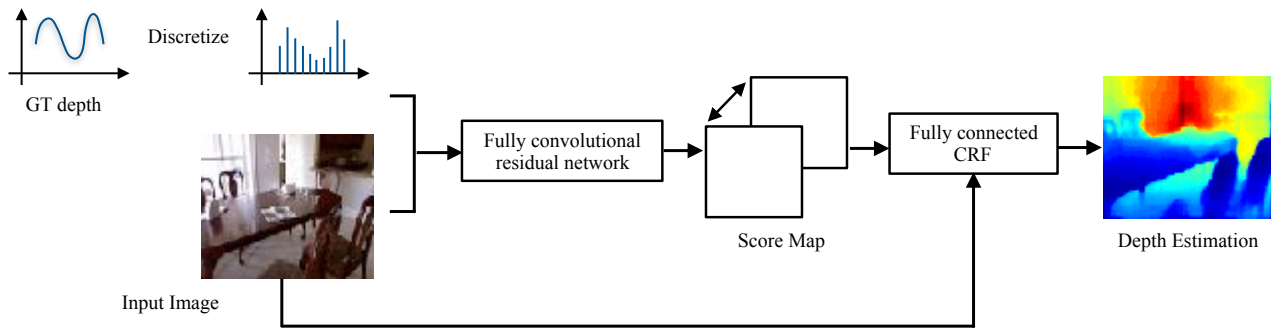


Fig. 1: An overview of our depth estimation model. It takes as input an image and output dense score maps. Fully-connected CRFs are then applied to obtain the final depth estimation.

also combined the CNNs with CRFs, they formulated depth estimation in a two-layer hierarchical CRF to enforce synergy between global and local predictions.

Anirban et al. [26] proposed a neural regression forest (NRF) architecture which combines convolutional neural networks with random forests for predicting depths in the continuous domain via regression. The NRF processes a data sample with an ensemble of binary regression trees and the final depth estimation is made by fusing the individual regression results. It allows for parallelizable training of all shallow CNNs, and efficient enforcing of smoothness in depth estimation results. Laina et al. [27] applied the deep residual networks for depth estimation. In order to improve the output resolution, they presented a novel way to efficiently learn feature map up-sampling within the network. They also presented a reverse Huber loss which is driven by the value distributions commonly present in depth maps for the network optimization.

Experiment results in the aforementioned works reveal that depth estimation benefits from: (a) an increased number of layers in deep networks; (b) obtaining fine-level details. In this work, we take advantage of the successful deep residual networks [14] and formulate depth estimation as a dense prediction task. We also apply fully connected CRFs [8] as post-processing. Although Laina et al. [27] also applied the deep residual network for depth estimation, our method is different from [27] in 3 distinct ways: Firstly, we formulate depth estimation as a classification task, while [27] formulated depth estimation as a regression task. Secondly, we can obtain the confidence of depth predictions which can be used during training and post-processing. Lastly, in order to obtain high resolution predictions, [27] applied an up-sampling scheme while we simply use bilinear interpolation.

The aforementioned CNN based methods formulate depth estimation as a structured regression task due to the continuous property of depth values. However for different pixels in a single monocular image, the possible depth values have different distributions. Depth values of some pixels are easy to predict while others are not. The output of continuous regression lacks this confidence. In [5], Pathak et al. presented a novel structured regression framework for image decomposition. It applied special constraints on the output space to capture the confidence of predictions. In [6], Kendall et al. proposed a

Bayesian neural network for semantic segmentation. It applied the Monte-Carlo dropout during training and obtained the confidence of predictions by multiple forward passes during evaluation. In this work, we obtain the confidence by simply formulating depth estimation as a classification task.

III. PROPOSED METHOD

In this section, we describe our depth estimation method in detail. We first introduce the network architecture, followed by the introduction of our loss function. Finally, we introduce the fully connected conditional random field (CRF) which is applied as post-processing.

A. Network architecture

We formulate our depth estimation as a spatially dense prediction task. When applying CNNs to this type of task, the input image is inevitably down-sampled due to the repeated combination of max-pooling and striding. In order to handle this, we follow the fully convolutional network (FCN) which has been proven to be successful in dense pixel labeling. It replaces the fully connected layers in conventional CNN architectures with convolutional layers. By doing this, it makes the fully convolutional networks capable of taking input of arbitrarily sized images and output a down-sampled prediction map. After applying a simple upsample such as bilinear interpolation, the prediction map is of the same size of the input image.

The depth of CNN architectures is of great importance. Much recent works reveal that the VGG [12] network outperforms the shallower AlexNet [11]. However, simply stacking more layers to existing CNN architectures does not necessarily improve performance due to the notorious problem of vanishing gradients, which hampers convergence from the beginning during training. The recent ResNet model solves this problem by adding skip connections. We follow the recent success of deep residual network with up to 152 layers [14], which is about $8\times$ deeper than the VGG network but still having fewer parameters to optimize.

Instead of directly learning the underlying mapping of a few stacked layers, the deep residual network learns the residual mapping. Then the original mapping can be realized by feedforward neural networks with “shortcut connections”.

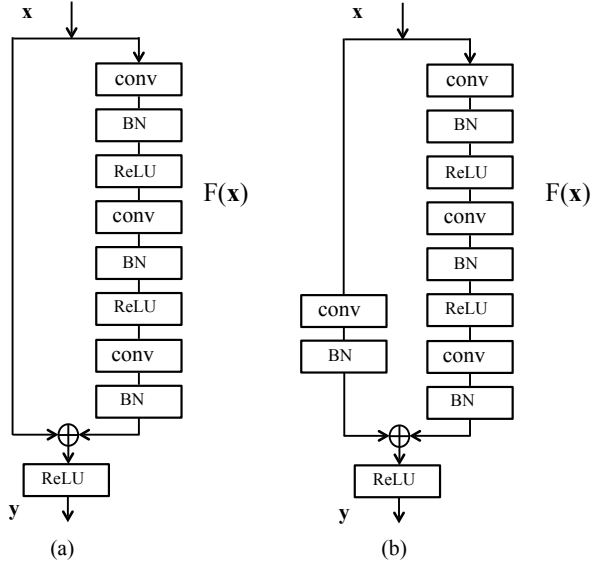


Fig. 2: Two types of building blocks that can be used in our depth estimation model. (a) building block with identity mapping. (b) building block with linear projection.

Shortcut connections are those skipping one or more layers. In our model, we consider two shortcut connections and the building blocks are shown in Fig. 2. The building block illustrated in Fig. 2(a) is defined as:

$$\mathbf{y} = F(\mathbf{x}, \{W_i\}) + \mathbf{x}, \quad (1)$$

where \mathbf{x} and \mathbf{y} are the input and output matrices of stacked layers respectively. The function $F(\mathbf{x}, \{W_i\})$ is the residual mapping that need to be learned. Since the shortcut connection is an element-wise addition, the dimensions of \mathbf{x} and F need to be same.

The building block illustrated in Fig. 2(b) is defined as:

$$\mathbf{y} = F(\mathbf{x}, \{W_i\}) + W_s \mathbf{x}. \quad (2)$$

Compared to the shortcut connection in Eq. (1), a linear projection W_s is applied to match the dimensions of \mathbf{x} and F .

The overall network architecture of our depth estimation model is illustrated in Fig. 3. The input image is fed into a convolutional layer, a max pooling layer followed by 4 convolution blocks. Each convolution block starts with a building block with linear projection followed by different numbers of building blocks with identity mapping. In this article, we consider two deep residual network architectures with 101 and 152 layers respectively. For the network architecture with 101 layers, the number of building blocks with identity mapping in the four convolution blocks (i.e., n_1, n_2, n_3, n_4 in Fig. 3) are 2, 3, 22 and 2 respectively. As for the network architecture with 152 layers, the numbers are 2, 7, 35 and 2. The last four layers are three convolutional layers with channels 1024, 512 and N , and a softmax layer, where N is the number of ground-truth labels. Batch normalization and ReLU layers are performed between these convolutional layers. Downsampling

is performed by pooling or convolutional layers that have a stride of 2. These include the first 7×7 convolutional layer, the first 3×3 max pooling layer, and the first building block of convolution block 2 in Fig. 3. As a result, the output prediction map is downsampled by a factor of 8. During prediction, we perform a bilinear interpolation on this map to make it the same size with the input image.

B. Loss function

In this work, we use the pixel-wise multinomial logistic loss function as we formulate depth estimation as a classification task. We uniformly discretize the continuous depth values into multiple bins in the log space. Each bin covers a range of depth values and we label the bins according to the range (i.e., the label index of a pixel indicates its distance). The depth labels however are different from the labels of typical classification tasks. For typical classification tasks such as semantic segmentation and object detection, the predictions that are different from ground-truth labels are considered wrong and contribute nothing in updating network parameters. As for depth estimation, the predictions that are close to ground-truth depth labels can also help in updating network parameters. This is achieved by an ‘‘information gain’’ matrix in our loss function.

Specifically, our loss function is defined as:

$$L = -\frac{1}{N} \sum_{i=1}^N \sum_{D=1}^B H(D_i^*, D) \log(P(D|z_i)), \quad (3)$$

where $D_i^* \in [1, \dots, B]$ is the ground-truth depth label of pixel i and B is the total number of discretization bins. $P(D|z_i) = e^{z_{i,D}} / \sum_{d=1}^B e^{z_{i,d}}$ is the probability of pixel i labelled with D . $z_{i,d}$ is the output of the last convolutional layer in the network. The ‘‘information gain’’ matrix H is a $B \times B$ symmetric matrix with elements $H(p, q) = \exp[-\alpha(p-q)^2]$ and α is a constant. It encourages the predicted depth labels that are closer to ground-truths have higher contributions in updating network parameters.

During prediction, we set the depth value of each pixel to be the center of its corresponding bin. By formulating depth estimation as classification, we can get the confidence of each prediction in the form of probability distribution. This confidence can also be applied during post-processing via fully connected CRFs.

C. Fully connected conditional random fields

A deep convolutional network typically does not explicitly take the dependency among local variables into consideration. It does so only implicitly through the field of view. That is why the size of field of view is important in terms of the performance of a CNN. In order to greatly refine the network output, we apply the fully connected CRF proposed in [8] as post-processing. It connects all pairs of individual pixels in the image. Specifically, the energy function of a fully connected CRF is the sum of unary potential U and pairwise potential V :

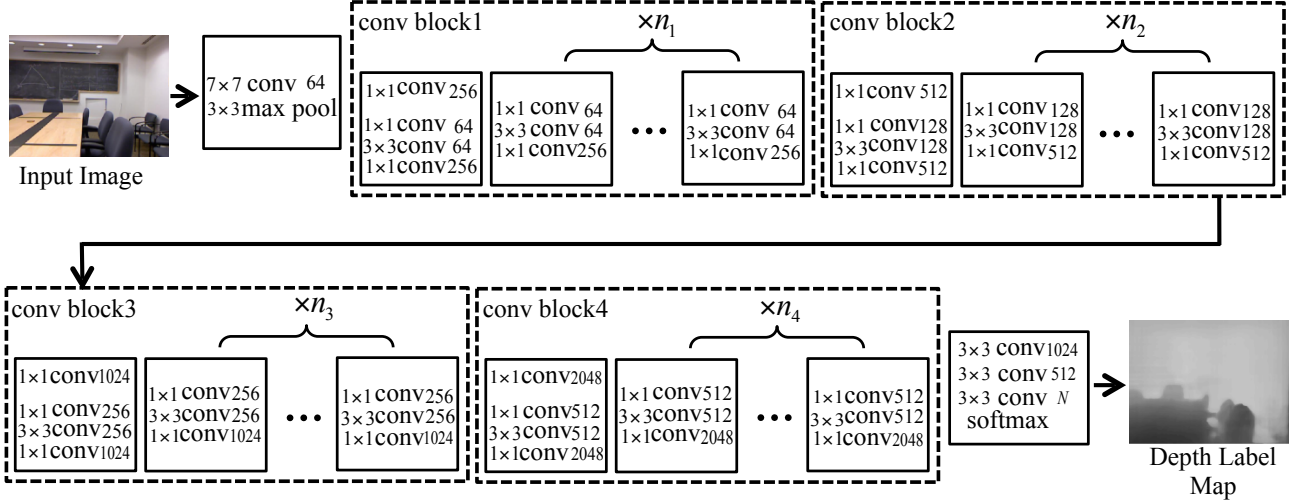


Fig. 3: Network architecture of our depth estimation model. The input image is fed into a convolutional layer, a max pooling layer and 4 convolution blocks. We consider network architectures with 101 and 152 layers. The value of $[n_1, n_2, n_3, n_4]$ is $[2, 3, 22, 2]$ for the 101-layer network architecture and $[2, 7, 35, 2]$ for the 152-layer network architecture. The last 4 layers are 3 convolutional layers and a softmax layer. The output map is downsampled by a factor of 8 and we perform bilinear interpolation during prediction.

$$E(\mathbf{D}) = \sum_i U(D_i) + \sum_{i,j} V(D_i, D_j), \quad (4)$$

where \mathbf{D} is the predicted depth labels of pixels and i, j are pixel indices. We use the logistic loss of pixel defined in Eq. (3) as the unary potential, which is

$$U(D_i) = L(D_i) = -\log(P(D_i|z_i)).$$

The pairwise potential is defined as

$$\sum_{i,j} V(D_i, D_j) = \Delta(D_i, D_j) \sum_{s=1}^M w_s \cdot k^s(\mathbf{f}_i, \mathbf{f}_j),$$

where $\Delta(D_i, D_j)$ is a penalty term on the labelling. Since the label here indicates depth, we enforce a relatively larger penalty for labellings that are far away from ground-truth. For simplicity, we use the absolute difference between two label values to be the penalty: $\Delta(D_i, D_j) = |D_i - D_j|$. There is one pairwise term for each pair of pixels in the image no matter how far they are from each other (i.e., the model's factor graph is fully connected).

Each k^s is the Gaussian kernel depends on features (denoted as \mathbf{f}) extracted for pixel i and j and is weighted by parameter w_s . Following [8], we adopt bilateral positions and color terms, specifically, the kernels are:

$$w_1 \exp\left(-\frac{\|p_i - p_j\|^2}{2\sigma_\alpha^2} - \frac{\|I_i - I_j\|^2}{2\sigma_\beta^2}\right) + w_2 \exp\left(-\frac{\|p_i - p_j\|^2}{2\sigma_\gamma^2}\right). \quad (5)$$

The first kernel is appearance kernel, which depends on both pixel positions (denoted as p) and pixel color intensities (denoted as I). It is inspired by the observation that nearby pixels with similar color are likely to be in the same depth

range. The degrees of nearness and similarity are controlled by hyper parameters σ_α and σ_β . The second kernel is smoothness kernel which removes small isolated regions, the scale of smoothness is controlled by σ_γ .

IV. EXPERIMENTS

We evaluate our proposed depth estimation approach on 2 benchmark RGB-D datasets: the indoor NYUD2 [28] dataset and the outdoor KITTI [29] dataset. We organize our experiments into the following three parts:

(1) We show the effectiveness of our depth discretization scheme and compare our discrete depth label classification with continuous depth value regression.

(2) We evaluate the contribution of different components in our proposed approach.

(3) We compare our proposed approach with state-of-the-art methods to show that our approach performs better in both indoor and outdoor scenes. Several measures commonly used in prior works are applied for quantitative evaluations:

- root mean squared error (rms): $\sqrt{\frac{1}{T} \sum_p (d_{gt} - d_p)^2}$
 - average relative error (rel): $\frac{1}{T} \sum_p \frac{|d_{gt} - d_p|}{d_{gt}}$
 - average log₁₀ error (log10): $\frac{1}{T} \sum_p |\log_{10} d_{gt} - \log_{10} d_p|$
 - root mean squared log error (rmslog): $\sqrt{\frac{1}{T} \sum_p (\log d_{gt} - \log d_p)^2}$
 - accuracy with threshold thr : percentage (%) of d_p s.t. $\max(\frac{d_{gt}}{d_p}, \frac{d_p}{d_{gt}}) = \delta < thr$
- where d_{gt} and d_p are the ground-truth and predicted depths respectively of pixels, and T is the total number of pixels in all the evaluated images.

A. Depth label classification vs. depth value regression

Discretizing continuous data would inevitably discard some information. In this part, we first show that the discretization of

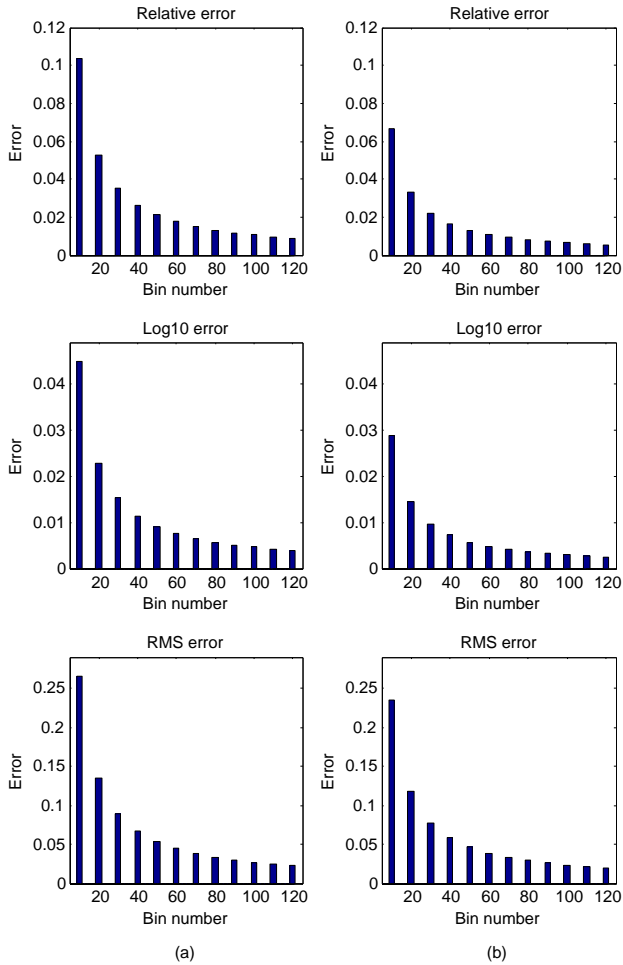


Fig. 4: *Quantitative evaluations of discretized ground-truth depth values of the NYUD2 dataset. (a): errors of ground-truth depth values discretized in linear space. (b): errors of ground-truth depth values discretized in the log space.*

continuous depth values degrades the depth estimation model by negligible amount. Specifically, we equally discretize the ground-truth depth values of test images in the NYUD2 dataset into different numbers of bins in the linear and log space respectively and calculate three errors as is mentioned above. The results are illustrated in Fig. 4.

We can see from Fig. 4 that with the increment of discretization bins, the errors of discretized ground-truth depths decrease and stop at a negligible amount. And the discretization in the log space leads to lower error than the discretization in the linear space.

As for the accuracies, all the discretized ground-truth depths can reach 100% except for the accuracy with threshold 1.25 when linearly discretizing the ground-truth depths into 10 bins. From this experiment we can see that converting the ground-truth depths from continuous values to discrete labels has negligible effect on the performance. We can reformulate depth estimation from a conventional regression task to a classification task.

TABLE I: *Depth estimation results by continuous depth value regression and discrete depth label classification for the NYUD2 and KITTI datasets. The first row is the result by regression. The following rows are results of depth label classification with different number of discretization bins.*

	Accuracy			Error		
	$\delta < 1.25$	$\delta < 1.25^2$	$\delta < 1.25^3$	rel	log10	rms
NYUD2						
Regression	65.3%	91.5%	97.4%	0.231	0.095	0.778
10 bins	69.4%	92.4%	97.5%	0.213	0.091	0.754
30 bins	70.5%	92.1%	97.8%	0.210	0.090	0.751
50 bins	68.9%	91.9%	97.0%	0.209	0.092	0.750
80 bins	70.6%	92.0%	97.6%	0.211	0.091	0.747
100 bins	70.1%	92.1%	97.3%	0.209	0.091	0.749
KITTI						
Regression	67.5%	88.6%	90.4%	0.279	0.104	7.916
50 bins	76.3%	92.1%	96.3%	0.183	0.077	6.209
80 bins	77.1%	91.7%	96.6%	0.180	0.072	6.311
120 bins	76.8%	91.9%	96.7%	0.187	0.076	6.263

We next compare our proposed depth estimation by classification with the conventional depth regression and show the results in Table I. In this experiment, we apply the deep residual network with 101 layers and the parameters are initialized with the ResNet101 model in [14] which is trained on the ImageNet classification dataset. We train our models on standard NYUD2 training set with 795 images and standard KITTI training set with 700 images [13] for fast comparison. As for the test sets, we select 650 and 700 images from the raw NYUD2 and KITTI test sets respectively as validation sets. For depth regression, the loss function is standard L_2 norm which minimizes the squared euclidean norm between predicted and ground-truth depths. The output depth map is upsampled to the same size of the input image through bilinear interpolation. As for our depth estimation by classification, we discretize the continuous depth values into different numbers of bins in the log space. We do not apply CRF post-processing for both regression and classification. As we can see from Table I that depth estimation by classification outperforms the conventional depth regression, and the performance of depth classification is not very sensitive to the number of discretization bins.

One important reason for depth estimation by classification outperforms the depth regression is that the regression tends to converge to the mean depth values. This may cause larger errors in areas that are either too far from or too close to the camera. The classification with the information gain may alleviate this problem. In order to testify this, we break down the NYUD2 ground-truth depths into 3 ranges and report the results in Table II. The general setting is the same with the aforementioned experiment. The ground-truth depths are discretized into 100 bins in the log space and the α defined in Eq. (3) is set to 0.2.

TABLE II: Test results on the NYUD2 dataset with different ground-truth ranges. We break down the ground-truth depths into 0m-3m, 3m-7m and 7m-10m.

	Accuracy			Error		
	$\delta < 1.25$	$\delta < 1.25^2$	$\delta < 1.25^3$	rel	log10	rms
	Regression					
0m-3m	65.7%	90.9%	97.4%	0.233	0.087	0.561
3m-7m	70.3%	95.5%	99.5%	0.175	0.075	0.936
7m-10m	45.0%	75.4%	93.5%	0.242	0.129	2.346
	Classification					
0m-3m	69.6%	91.2%	97.2%	0.216	0.083	0.561
3m-7m	76.0%	94.9%	98.6%	0.151	0.070	0.857
7m-10m	49.7%	74.9%	93.1%	0.238	0.126	2.199

TABLE III: Test results on the NYUD2 and KITTI datasets with and without information gain matrices. For each dataset, the first row is the result without information gain matrix, the second row is the result with information gain matrix.

	Accuracy			Error		
	$\delta < 1.25$	$\delta < 1.25^2$	$\delta < 1.25^3$	rel	log10	rms
	NYUD2					
Plain	70.9%	92.1%	98.0%	0.193	0.079	0.716
Infogain	72.2%	92.6%	98.0%	0.192	0.077	0.688
	KITTI					
Plain	79.9%	93.7%	97.6%	0.166	0.067	5.443
Infogain	81.4%	93.9%	97.6%	0.153	0.062	5.290

B. Component evaluation

In this section, we analyze the contribution of key components including the information gain matrix, fully connected CRFs and network architectures in our proposed approach. We evaluate depth estimation on both the NYUD2 and KITTI datasets. We use the standard training set containing 795 images of the NYUD2 dataset and evaluate on the standard 654 test images. The continuous depth values are discretized into 100 bins in the log space. As for the KITTI dataset, we apply the same split in [13] which contains 700 training images and 697 test images. We only use left images and discretize the continuous depth values into 50 bins in the log space. We cap the maximum depth to be 80 meters. During training, we ignore the missing values in ground-truth depths and only evaluate on valid points.

1) *Benefit of information gain matrix:* In this part, we evaluate the contribution of the information gain matrix in our loss function. We train the ResNet101 model on both the NYUD2 and KITTI datasets with and without information gain matrices. The α defined in Eq. (3) is set to 0.2 and 0.5 for NYUD2 and KITTI respectively. In our experiments, we find that the performance is not sensitive to α . The results are illustrated in Table III. As we can see from this table that the information gain matrix improves the performance of both indoor and outdoor depth estimation.

2) *Benefit of fully connected CRFs:* In order to evaluate the effect of the fully connected CRFs, we first train the

TABLE IV: Test results on the NYUD2 and KITTI datasets with and without the fully connected CRFs as post-processing. For each dataset, the first row is the result without CRFs, the following row is the result with CRFs.

	Accuracy			Error		
	$\delta < 1.25$	$\delta < 1.25^2$	$\delta < 1.25^3$	rel	log10	rms
	NYUD2					
Plain	70.9%	92.1%	98.0%	0.193	0.079	0.716
CRF	71.3%	92.0%	98.0%	0.190	0.079	0.696
	KITTI					
Plain	79.9%	93.7%	97.6%	0.166	0.067	5.443
CRF	81.0%	94.1%	97.9%	0.167	0.066	5.349

TABLE V: Test results on the NYUD2 dataset with different network structures. The first row is the result of the VGG16 net, the following two rows are the results of deep residual networks. We also show the total number of parameters of the three networks in the last row.

	Accuracy			Error		
	$\delta < 1.25$	$\delta < 1.25^2$	$\delta < 1.25^3$	rel	log10	rms
VGG16	62.1%	87.2%	96.0%	0.236	0.097	0.857
ResNet101	70.9%	92.1%	98.0%	0.193	0.079	0.716
ResNet152	71.2%	92.3%	98.0%	0.187	0.071	0.681
	VGG16		ResNet101	ResNet152		
Parameters	13.9×10^7		6.7×10^7	8.2×10^7		

ResNet101 model on both the NYUD2 and KITTI datasets, and then apply the fully connected CRFs as post-processing. We illustrate the results in Table IV. As we can see from the table, the fully-connected CRF can improve the depth estimation of both indoor and outdoor scenes.

3) *Network Comparisons:* In this part, we compare the performance of deep residual networks with the baseline VGG16 net [12] on the NYUD2 dataset. Since we formulate depth estimation as a classification task, we can apply network structures that perform well on semantic segmentation task. Specifically, for the VGG16 net, we apply the structure in [9]. We keep the layers up to “fc6” in VGG16 net and add 2 convolutional layers with 512 channels, and 2 fully-connected layers with 512 and 100 channels respectively. The results are illustrated in Table V. The performance of residual networks unsurprisingly outperform the VGG16 net, reinforcing the importance of network depth. Note that the performance by the ResNet152 improves little to the ResNet101, this is caused by the overfitting as the training set contains only 795 images. We also compare the number of parameters in the Table V.

C. State-of-the-art comparisons

In this section, we evaluate our approach on the NYUD2 and KITTI datasets and compare with recent depth estimation methods. We apply the deep residual network with 152 layers and the parameters are initialized with the ResNet152 model in [14].

TABLE VI: Comparison with state-of-the-art on the NYUD2 dataset. The first 4 rows are results by recent depth estimation models. The last row is the result of our approach.

	Accuracy			Error		
	$\delta < 1.25$	$\delta < 1.25^2$	$\delta < 1.25^3$	rel	log10	rms
Wang et al. [3]	60.5%	89.0%	97.0%	0.210	0.094	0.745
Liu et al. [4]	65.0%	90.6%	97.6%	0.213	0.087	0.759
Anirban et al. [26]	-	-	-	0.187	0.078	0.744
Eigen et al. [1]	76.9%	95.0%	98.8%	0.158	-	0.641
Laina et al. [27]	81.1%	95.3%	98.8%	0.127	0.055	0.573
Ours	81.9%	96.5%	99.2%	0.141	0.060	0.540

TABLE VII: Comparison with state-of-the-art results on the KITTI dataset. We cap the maximum depth to 50 and 80 meters to compare with recent works. For the work in [30], we also report their results with additional training images in the CityScapes dataset [31] and denote as Godard et al. CS.

	Accuracy			Error		
	$\delta < 1.25$	$\delta < 1.25^2$	$\delta < 1.25^3$	rel	rmslog	rms
Cap 80 meters						
Liu et al. [4]	65.6%	88.1%	95.8%	0.217	-	7.046
Eigen et al. [13]	69.2%	89.9%	96.7%	0.190	0.270	7.156
Godard et al. [30]	81.8%	92.9%	96.6%	0.141	0.242	5.849
Godard et al. CS [30]	83.6%	93.5%	96.8%	0.136	0.236	5.763
Ours	88.7%	96.3%	98.2%	0.115	0.198	4.712
Cap 50 meters						
Garg et al. [32]	74.0%	90.4%	96.2%	0.169	0.273	5.104
Godard et al. [30]	84.3%	94.2%	97.2%	0.123	0.221	5.061
Godard et al. CS [30]	85.8%	94.7%	97.4%	0.118	0.215	4.941
Ours	89.8%	96.6%	98.4%	0.107	0.187	3.605

1) *NYUD2*: We train our model using the entire raw training data specified in the official train/test distribution and test on the standard 654 test images. We discretize the depth values into 100 bins in the log space. We set the parameter α of the information gain matrix to be 0.2. The fully connected CRFs are applied as post-processing. The results are reported in Table VI. The first row is the result in [3] which jointly performs depth estimation and semantic segmentation. The second row is the result of deep convolutional neural fields (DCNF) with fully convolutional network and super-pixel pooling in [4]. The third row is the result of neural regression forest (NRF) in [26]. The fourth row is the result in [1] which performs depth estimation in a multi-scale network architecture. The fifth row is the result in [27] which applies an upsampling scheme. The last row is depth estimation result by our model. As we can see from the table, our deep fully convolutional residual network with depth label classification achieves state-of-the-art performance of 4 evaluation metrics. We also show some qualitative results in Fig. 5, from which we can see our method yields better visualizations in general.

2) *KITTI*: We train our model on the same training set in [30] which contains 33131 images and test on the same 697 images in [13]. But different from the depth estimation method proposed in [30] which applies both the left and right images in stereo pairs, we only use the left images. The missing values in the ground-truth depth maps are ignored during both training and evaluation. The depth values are discretized into 50 bins in the log space. We set the parameter α of the information gain matrix to be 0.5 and apply fully connected CRFs as post-

TABLE VIII: Test results on the SUN RGB-D dataset for cross-dataset evaluation. The first 2 rows are results by recent depth estimation models. The last row is the result of our approach.

	Accuracy			Error		
	$\delta < 1.25$	$\delta < 1.25^2$	$\delta < 1.25^3$	rel	log10	rms
Liu [4]	35.6%	57.6%	83.1%	0.316	0.161	0.931
Laina [27]	53.9%	70.3%	89.0%	0.279	0.138	0.851
Ours	56.3%	72.7%	88.2%	0.256	0.127	0.839

processing. In order to compare with the recent state-of-the-art results, we cap the maximum depth into both 80 meters and 50 meters and present the results in Table VII. We can see from Table VII that our method outperforms the rest methods significantly. Some qualitative results are illustrated in Fig. 6. Our approach yields visually better results.

3) *Cross-dataset evaluation*: In order to show the generalization of our proposed method, we train our model on the raw NYUD2 dataset and test on the SUN RGB-D dataset [33]. The SUN RGB-D is an indoor dataset contains 10335 RGB-D images captured by four different sensors. We only select 500 images randomly from the test set for cross-dataset evaluation. The SUN RGB-D contains 1449 images from the NYUD2 dataset. Our selected testset excludes all the images from the NYUD2. We compare our method with Liu et al. [4] and Laina et al. [27]. We use the trained models and evaluation codes released by these authors. The results are illustrated in Table VIII. We can see that our method can reach satisfactory

results on different dataset, and outperforms other methods.

V. CONCLUSION

We have presented a deep fully convolutional residual network architecture for depth estimation from single monocular images. We have made use of the recent deep residual networks, discretized continuous depth values into different bins and formulated depth estimation as a discrete classification problem. By this formulation we can easily obtain the confidence of a prediction which can be applied during training via information gain matrices as well as post-processing via fully-connected CRFs. We have shown that our discretization approach surprisingly performs well.

Note that the proposed network can be further improved by applying the techniques that have been previously explored. For example, it is expected that

- Multi-scale inputs as in [1] would improve our result.
- Concatenating the mid-layers' outputs may better use the low-, mid-layers information as in [34].
- Upsampling the prediction maps as in [35] would be beneficial too.

We leave these directions in our future work.

REFERENCES

- [1] D. Eigen and R. Fergus, "Predicting depth, surface normals and semantic labels with a common multi-scale convolutional architecture," in *Proc. IEEE Int. Conf. Comp. Vis.*, 2015.
- [2] B. Li, C. Shen, Y. Dai, A. van den Hengel, and M. He, "Depth and surface normal estimation from monocular images using regression on deep features and hierarchical CRFs," in *Proc. IEEE Conf. Comp. Vis. Patt. Recogn.*, 2015.
- [3] P. Wang, X. Shen, Z. Lin, S. Cohen, B. Price, and A. L. Yuille, "Towards unified depth and semantic prediction from a single image," in *Proc. IEEE Conf. Comp. Vis. Patt. Recogn.*, June 2015.
- [4] F. Liu, C. Shen, G. Lin, and I. D. Reid, "Learning depth from single monocular images using deep convolutional neural fields," *IEEE Trans. Pattern Anal. Mach. Intell.*, 2016.
- [5] D. Pathak, P. Krähenbühl, S. X. Yu, and T. Darrell, "Constrained structured regression with convolutional neural networks," 2016. [Online]. Available: <http://arxiv.org/abs/1511.07497>
- [6] A. Kendall, V. Badrinarayanan, and R. Cipolla, "Bayesian SegNet: Model uncertainty in deep convolutional encoder-decoder architectures for scene understanding," 2015. [Online]. Available: <http://arxiv.org/abs/1511.02680>
- [7] Y. Gal and Z. Ghahramani, "Bayesian convolutional neural networks with Bernoulli approximate variational inference," 2016.
- [8] P. Krähenbühl and V. Koltun, "Efficient inference in fully connected CRFs with gaussian edge potentials," in *Proc. Adv. Neural Inf. Process. Syst.*, 2011.
- [9] G. Lin, C. Shen, I. D. Reid, and A. van den Hengel, "Efficient piecewise training of deep structured models for semantic segmentation," in *Proc. IEEE Conf. Comp. Vis. Patt. Recogn.*, 2016.
- [10] L. Chen, G. Papandreou, I. Kokkinos, K. Murphy, and A. L. Yuille, "Semantic image segmentation with deep convolutional nets and fully connected CRFs," *Proc. IEEE Int. Conf. Learn. Rep.*, 2015.
- [11] A. Krizhevsky, I. Sutskever, and G. E. Hinton, "Imagenet classification with deep convolutional neural networks," in *Proc. Adv. Neural Inf. Process. Syst.*, 2012, pp. 1097–1105.
- [12] K. Simonyan and A. Zisserman, "Very deep convolutional networks for large-scale image recognition," *Proc. Int. Conf. Learn. Rep.*, 2015.
- [13] D. Eigen, C. Puhrsch, and R. Fergus, "Depth map prediction from a single image using a multi-scale deep network," in *Proc. Adv. Neural Inf. Process. Syst.*, 2014.
- [14] K. He, X. Zhang, S. Ren, and J. Sun, "Deep residual learning for image recognition," in *Proc. IEEE Conf. Comp. Vis. Patt. Recogn.*, 2016.
- [15] V. Hedau, D. Hoiem, and D. Forsyth, "Thinking inside the box: Using appearance models and context based on room geometry," in *Proc. Eur. Conf. Comp. Vis.*, 2010, pp. 224–237.
- [16] A. Gupta, M. Hebert, T. Kanade, and D. M. Blei, "Estimating spatial layout of rooms using volumetric reasoning about objects and surfaces," in *Proc. Adv. Neural Inf. Process. Syst.*, 2010.
- [17] A. G. Schwing and R. Urtasun, "Efficient exact inference for 3d indoor scene understanding," in *Proc. Eur. Conf. Comp. Vis.*, 2012.
- [18] K. Karsch, C. Liu, and S. B. Kang, "Depthtransfer: Depth extraction from video using non-parametric sampling," *IEEE Trans. Pattern Anal. Mach. Intell.*, 2014.
- [19] B. C. Russell and A. Torralba, "Building a database of 3d scenes from user annotations," in *Proc. IEEE Conf. Comp. Vis. Patt. Recogn.*, 2009.
- [20] B. Liu, S. Gould, and D. Koller, "Single image depth estimation from predicted semantic labels," in *Proc. IEEE Conf. Comp. Vis. Patt. Recogn.*, 2010.
- [21] L. Ladicky, J. Shi, and M. Pollefeys, "Pulling things out of perspective," in *Proc. IEEE Conf. Comp. Vis. Patt. Recogn.*, 2014.
- [22] A. Saxena, A. Ng, and S. Chung, "Learning Depth from Single Monocular Images," *Proc. Adv. Neural Inf. Process. Syst.*, 2005.
- [23] A. Saxena, M. Sun, and A. Y. Ng, "Make3D: Learning 3d scene structure from a single still image," *IEEE Trans. Pattern Anal. Mach. Intell.*, 2009.
- [24] A. Saxena, S. H. Chung, and A. Y. Ng, "3-d depth reconstruction from a single still image," *Int. J. Comp. Vis.*, 2007.
- [25] M. Liu, M. Salzmann, and X. He, "Discrete-continuous depth estimation from a single image," in *Proc. IEEE Conf. Comp. Vis. Patt. Recogn.*, 2014.
- [26] A. Roy and S. Todorovic, "Monocular depth estimation using neural regression forest," in *Proc. IEEE Conf. Comp. Vis. Patt. Recogn.*, 2016.
- [27] I. Laina, C. Rupprecht, V. Belagiannis, F. Tombari, and N. Navab, "Deeper depth prediction with fully convolutional residual networks," in *Proc. IEEE Int. Conf. 3D Vision*, October 2016.

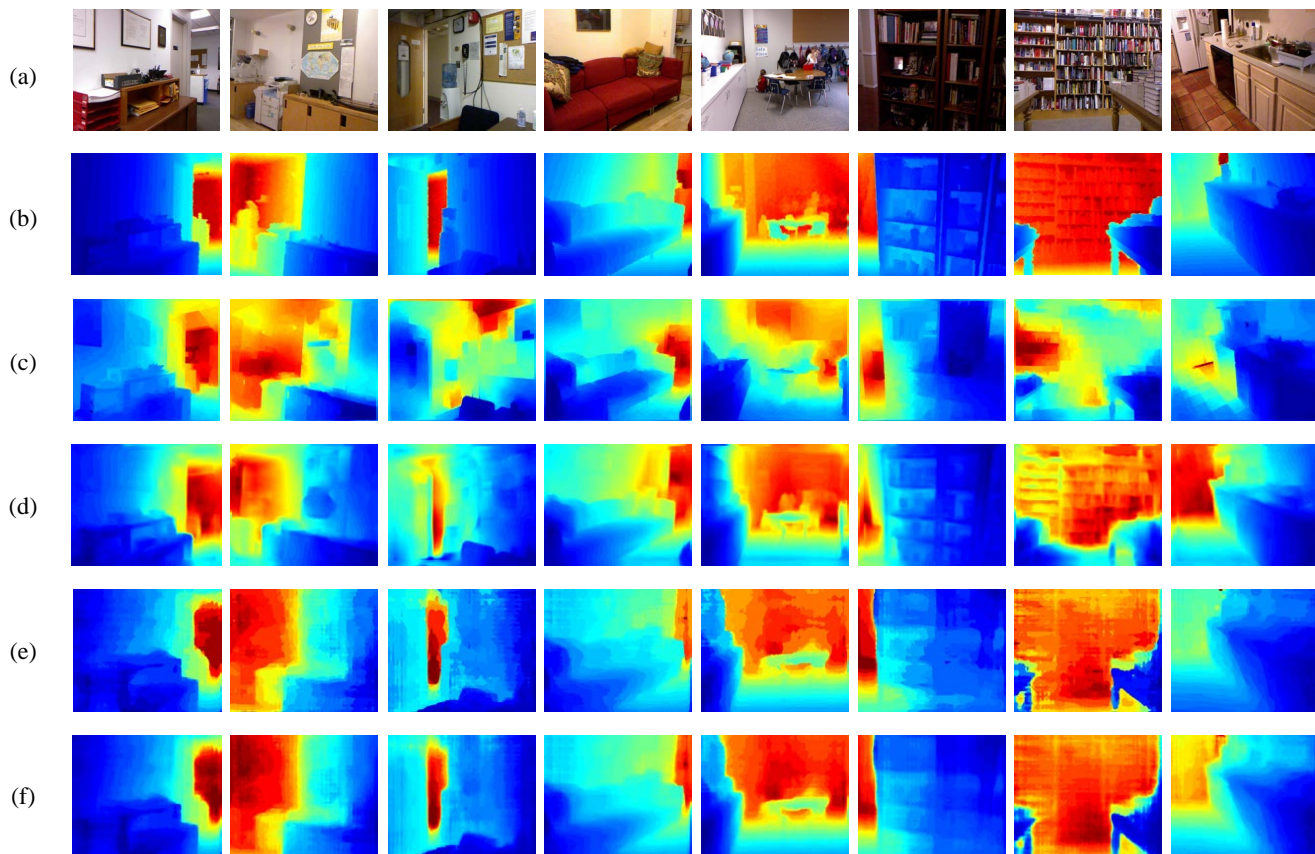


Fig. 5: Some depth estimation results on the NYUD2 dataset. (a) RGB Input; (b) Ground-truth depth; (c) Results of Liu et al. [4]; (d) Results of Eigen et al. [1]; (e) Results of our model without fully-connected CRFs; (f) Results of our model with fully-connected CRFs.

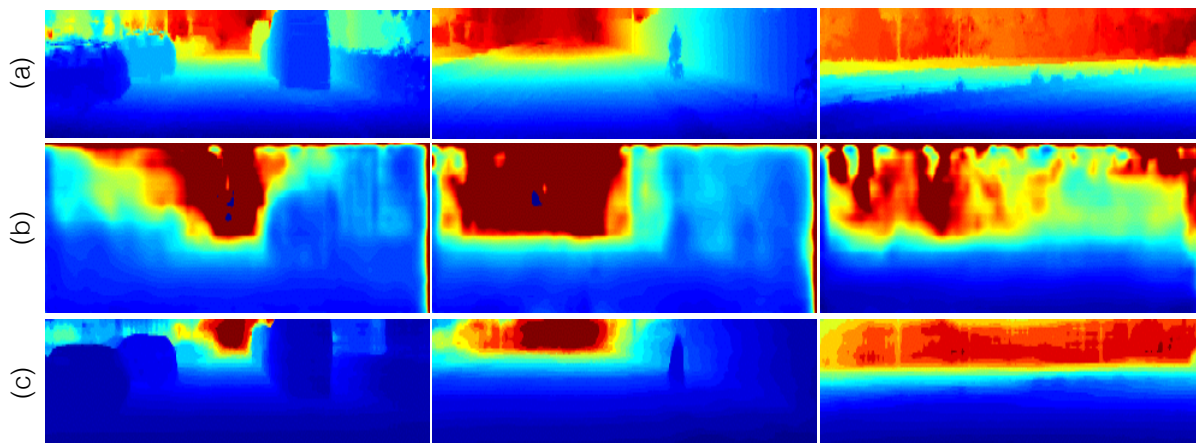


Fig. 6: Some depth estimation results of the KITTI dataset. The first row are the ground-truth depths, the second row are the results by [32], the last row are the results by our approach.

- [28] N. Silberman, D. Hoiem, P. Kohli, and R. Fergus, "Indoor segmentation and support inference from rgb-d images," in *Proc. Eur. Conf. Comp. Vis.*, 2012.
- [29] A. Geiger, P. Lenz, C. Stiller, and R. Urtasun, "Vision meets robotics: The kitti dataset," *Int. J. Robt. Res.*, 2013.
- [30] C. Godard, O. Mac Aodha, and G. J. Brostow, "Unsupervised monocular depth estimation with left-right consistency," 2016. [Online]. Available: <https://arxiv.org/pdf/1609.03677v1.pdf>
- [31] M. Cordts, M. Omran, S. Ramos, T. Rehfeld, M. Enzweiler, R. Benenson, U. Franke, S. Roth, and B. Schiele, "The cityscapes dataset for semantic urban scene understanding," in *Proc. IEEE Conf. Comp. Vis. Patt. Recogn.*, 2016.
- [32] R. Garg and I. Reid, "Unsupervised cnn for single view depth estimation: Geometry to the rescue," in *Proc. Eur. Conf. Comp. Vis.*, 2016.
- [33] S. Song, S. P. Lichtenberg, and J. Xiao, "SUN RGB-D: A rgb-d scene understanding benchmark suite," in *Proc. IEEE Conf. Comp. Vis. Patt. Recogn.*, 2015.
- [34] B. Hariharan, P. Arbeláez, R. Girshick, and J. Malik, "Hypercolumns for object segmentation and fine-grained localization," in *Proc. IEEE Conf. Comp. Vis. Patt. Recogn.*, 2015.
- [35] J. Long, E. Shelhamer, and T. Darrell, "Fully convolutional networks for semantic segmentation," *Proc. IEEE Conf. Comp. Vis. Patt. Recogn.*, 2015.